COMMUNICATION

Particulate gel liquid marbles†

Mizuki Tenjimbayashi,*[a,b] Ryota Tamate[c]

Received 00th January 20xx,
Accepted 00th January 20xx

DOI: 10.1039/x0xx00000x

Nonsticking water droplets stabilized by particulate polydimethylsiloxane (PDMS) organogel, namely "particulate gel liquid marbles (PGLMs)" are prepared *via* mechanochemistry. PGLM exhibited superior compression/impact stability to conventional particle-stabilized LM owing to the organogel rheological feature. Moreover, the shape reconfigurability of PG enabled the plastic deformation of PGLMs.

The design of liquid non-sticking surfaces/interfaces is of great interest owing to their anti-fouling and self-cleaning functions.[1] Hydrophobic nano/micro textures prevent the sticking of water droplet and a contacting substrate by forming the Cassie-Baxter interface,[2] which entraps the air layer beneath the droplet and minimizes the droplet contact area. On one hand, the structure is fixed on the substrate, and the surface exhibits superhydrophobicity. On the other hand, when the hydrophobic texture is formed on the droplet by adsorption of hydrophobic fine particles, the non-sticking droplet is recognized as liquid marble (LM).[3]

LM has been intensively studied due to its unique properties since the first report in 2001.[4] LM behaves like a soft solid but is reconfigurable (e.g., splitting and coalescing) like liquid. Moreover, LMs roll off the tilted substrate or float on the water pool. These properties enabled loss-less inner liquid transportation and easy recyclability of outer particles. Thus, LMs are expected to use sustainable materials for transportation. Various lab-in-a-marble applications have been considered by replacing the inner liquid with a responsive one with chemicals, sensing molecules, and cells.[3] Moreover, functional/responsive particles covering the droplet make the applications more convenient.[5]

However, LM is mechanically weak because the hydrophobic particle texture on the droplet is discontinuous, and mechanical stimuli induce cracking or inner liquid penetration.[6] Thus, various works focused on the mechanical durability of LM. Compression and/or impact stability of LM in changing the possible parameters: particle size or shape, droplet size,

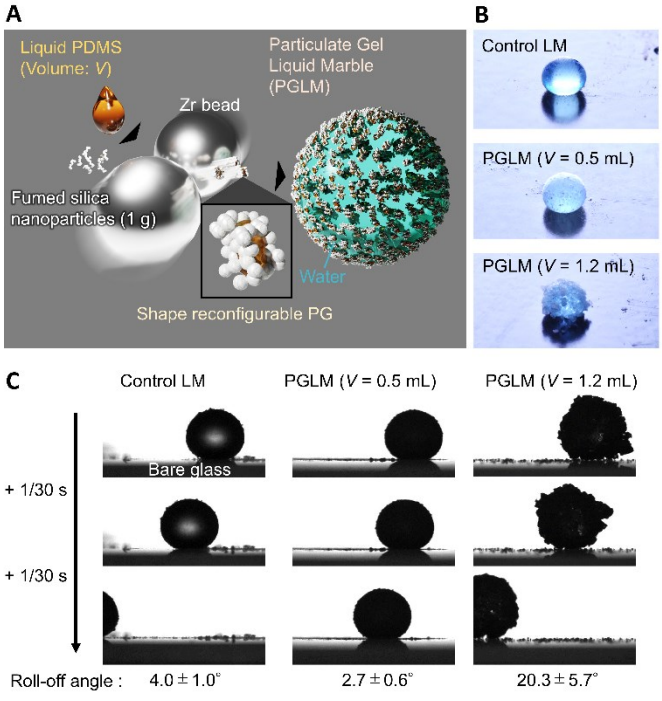

Figure 1. (A) Design strategy of PG and PGLM (B, C) Photo images of classical LM and PGLMs in (B) resting and (C) rolling-off on the tilted glass substrate. Water volume is 10 μL in constant. Rolling-off angle tends to increase with the roughness of the PGLMs.

[a] *Research Center for Materials Nanoarchitectonics (MANA), National Institute for Materials Science (NIMS), 1-1 Namiki, Tsukuba, Ibaraki 305-0044, Japan.*
[b] *FOREST, Japan Science and Technology Agency, Saitama 332-0012, Japan.*
** E-mail: TENJIMBAYASHI.Mizuki@nims.go.jp.*
[c] *Research Center for Macromolecules & Biomaterials, NIMS, 1-2-1 Sengen, Tsukuba, 305-0047, Japan.*
†Electronic Supplementary Information (ESI) available: [details of any supplementary information available should be included here]. See DOI: 10.1039/x0xx00000x

viscosity, or surface tension, contacting substrate wettability, on/under water conditions, have been investigated.[7–13] However, we still suffer from LM fragility. Ideas to polymerize the hydrophobic texture of LM have also been reported; however, the interfacial polymerization loses the reconfigurability of LM.[14]

Recently, various new concepts of LMs have been reported. Pritam et al. reported LM, whose particle layer is impregnated by the lubricant.[15] Aono et al. reported that the LM was made of droplet-shaped foam.[16] Takei et al. reported LM, whose particles are made of hydrophobic gelatine.[17] These researchers succeeded in tethering a sister fluid phase (infusing liquid, bubble, or gel) in the LM system. We hypothesize that the sister fluid can dissipate the mechanical stimuli owing to its viscous effect, potentially modulating the mechanical stability of LMs.

Here, we designed the LM made of water droplets covering PG, namely PGLM (**Figures 1A** and **1B**). The PGLMs exhibit non-sticking rolling-off behaviors on tilted glass substrates like classical LMs (**Figure 1C**). The PG consists of a percolated network of fumed silica nanoparticles whose primary diameter is ~7 nm (AEROSIL® 300, Evonik Industries, Germany) in liquid PDMS with a viscosity of 10^5 mPa s (**Figure S1**). It is known that the mechano-chemical process enables the modification of PDMS in silica nanoparticles.[18] We added an excess amount of liquid PDMS in mechano-chemical processes and succeeded in forming PG particles. This work studies the effect of PDMS volume fraction on PG structure and PGLM mechanical property. As a result, the PGLM exhibits higher resilience and mechanical stability than LM covered with commercial PDMS-modified fumed silica nanoparticles (AEROSIL® RY300, Evonik Industries, Germany) as control, opening a new door to a robust LM design strategy.

Moreover, the PG exhibits shape reconfiguration property and tethers mechano-adaptivity to PGLMs. We expect the PGLM to evolve from classical "responsive" to "adaptive" LMs. The PG process is universal to various viscous liquids and thus potentially diversifies the sister liquid-based LM system.

Figure 2A explains the effect of the liquid PDMS volume on PG structures. While AEROSIL® 300 weight is kept at 1 g, liquid PDMS volume V varies from 0 to 1.5 mL. PG grows with the increase in the PDMS volume. Because the fumed silica nanoparticles are wet by liquid PDMS, the liquid PDMS capillary work isotopically wet the nanoparticles. However, the bulk elasticity limits the spill of the PDMS from nanoparticle networks. **Figure 2B** visualizes the PG structures and AEROSIL® 300 as a comparison using digital microscopy. Due to the electrostatic force, the AEROSIL® 300 is in a semi-transparent micrometer aggregate state. However, PDMS-added grains are white-colored ones. The differences in transparency depend on whether or not PDMS is infused in the nanoparticle network. The tendency is observed for the comparison between control LM and PGLMs (**Figure 1B**). We measured the short (long) diameters a (b) of grains from these images. Then, the grain diameter $D = (a+b)/2$ and the sphericity $\Psi = a/b$ are obtained **(Figure 2C)**. As shown in **Figure 2D**, while the diameter is nearly

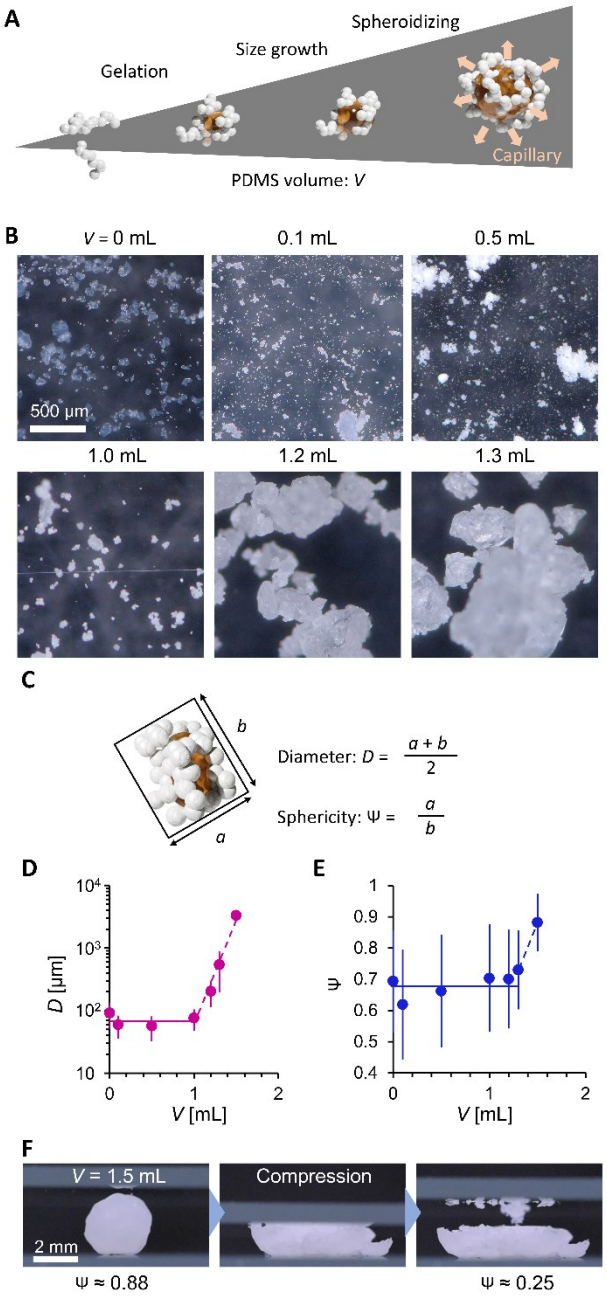

Figure 2. (A) PDMS volume effect on PG. (B) Digital microscopic images (C) Scheme explaining PG geometry analysis. (D) Diameter and (E) sphericity of PG. (F) Mechcanical shape reconfiguration of PG.

constant till V = 1 mL, it exponentially increased from tens μm to mm in range with varying V from 1 to 1.5 mL. The D increase can be explained by the PDMS sticking the nanoparticles to grow up. We assume the constant diameter in $V < 1$ mL is owing to the competition of the particles' mechanical cracking for decreasing size and PDMS sticking for increasing. The diameter error is negligible since the ball milling makes the grains uniform (see the histograms in **Figure S2**). **Figure 2E** shows that the sphericity remains constant at ~0.7 except V = 1.5 mL. The high sphericity in V = 1.5 mL can be explained by the surface tension

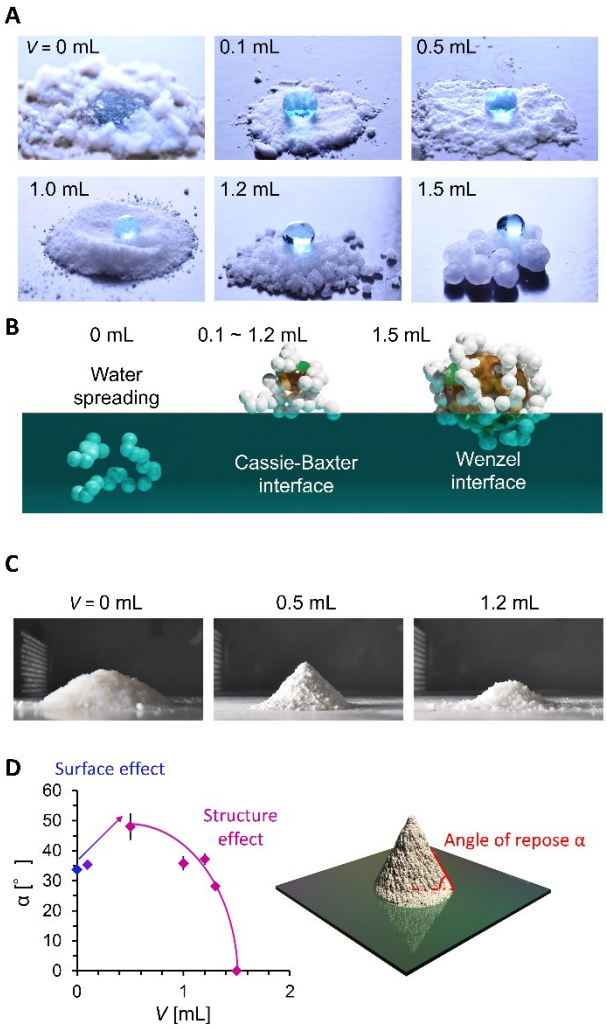

Figure 3. (A) 20 µL Water droplets on PG. (B) Water adhesion states on PG estimated from water contact behaviors. (C) Shape of particle or PG powder mountain. (D) Angle of repose evolution.

effect which strengthens with the liquid PDMS amount. Unlike the classical LMs that use (elastic) solid particles, the PG plastically deforms due to the unfixed particulate network. Thus, the PG can transform its shape through mechanical compression. Such reconfigurable particles have not been applied in LMs. In **Figure 2F**, simple compression transforms the PG from sphere to plate.

We then evaluated the wettability and powder fluidity of PGs in **Figure 3**. **Figure 3A** shows the photo images of the water droplets on grain beds. While water spread on hydrophilic AEROSIL® 300 (*V*=0) bed, the bed by PDMS included grains (*V* = 0.1 to 1.2 mL) exhibit superhydrophobic negligibly small sticking behaviors against 20 µL water droplets. The droplet on PG with *V* = 1.5 mL exhibited a high contact angle but stuck to the PG surface (see **Figure S3**). Such wettability variation is due to the different wetting states (**Figure 3B**). Although the accurate water contact angle on the powder bed is difficult, the wetting states are easily judged from the water adhesion behavior.[6] In *V*=0, water is entrapped between the nanoparticles owing to the intrinsic hydrophilicity of AEROSIL® 300. In *V* ranges from 0.1 to 1.2 mL, the water cannot invade between the nanoparticles owing to the hydrophobicity from PDMS modification; instead, the air is entrapped beneath the water droplet, forming the Cassie-Baxter interface. Notably, the 0.1 mL of PDMS is enough to hydrophobize AEROSIL® 300. For *V* = 0.5 to 1.2mL, liquid PDMS is entrapped in the nanoparticles while forming a Cassie-Baxter interface with water. This means that the liquid PDMS is insufficient to cover the surface nanoparticles of the grains.[19] In *V* = 1.5 mL, the water in the Wenzel state sticks to the PG mediated by surface partially exposed liquid PDMS.

We then evaluated the powder fluidity of PGs via the angle of the repose α measurement (**Figure 3C** and **3D**). In general, α increases with the friction between grains (i.e., surface effect) or decreases in *D* and Ψ (i.e., structure effect). We observed α increases with *V* from 0, 0.1, to 0.5 mL while the constant *D* and increased Ψ (**Figures 2D** and **2E**). It means

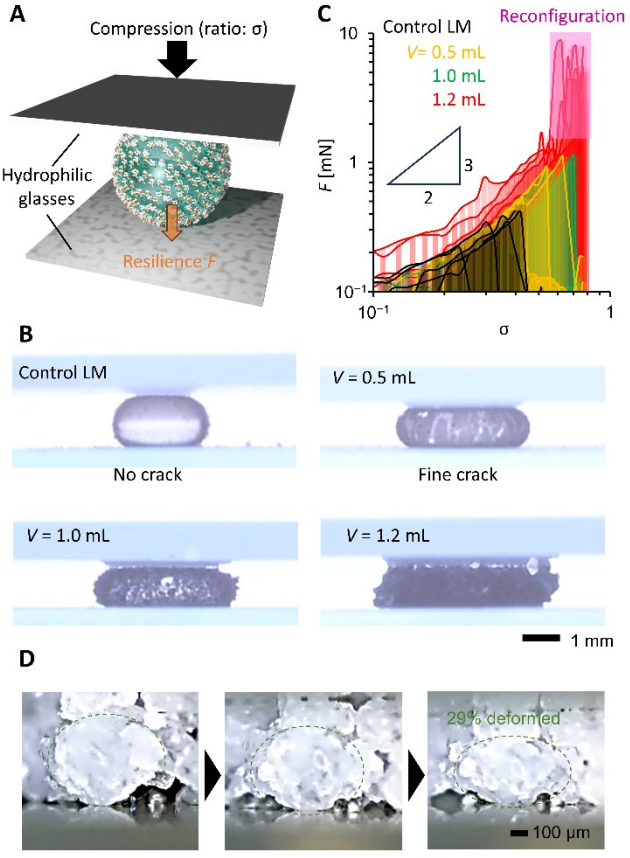

Figure 4. (A) Scheme of the compression test. (B) Side view of compressed PGLM just before breakage with 10µL water. (C) Compression-resilience curve of PGLM with 10µL water in different PDMS volume. Resilience fluctuation region (Pink highlighted) is owing to the PG reconfiguration. (D) Side-view microscopic image monitoring the deformation of the PG (*V* = 1.2 mL) in the deformation of PGLM by a glass plate. The observed PG deformed by around 29% in height.

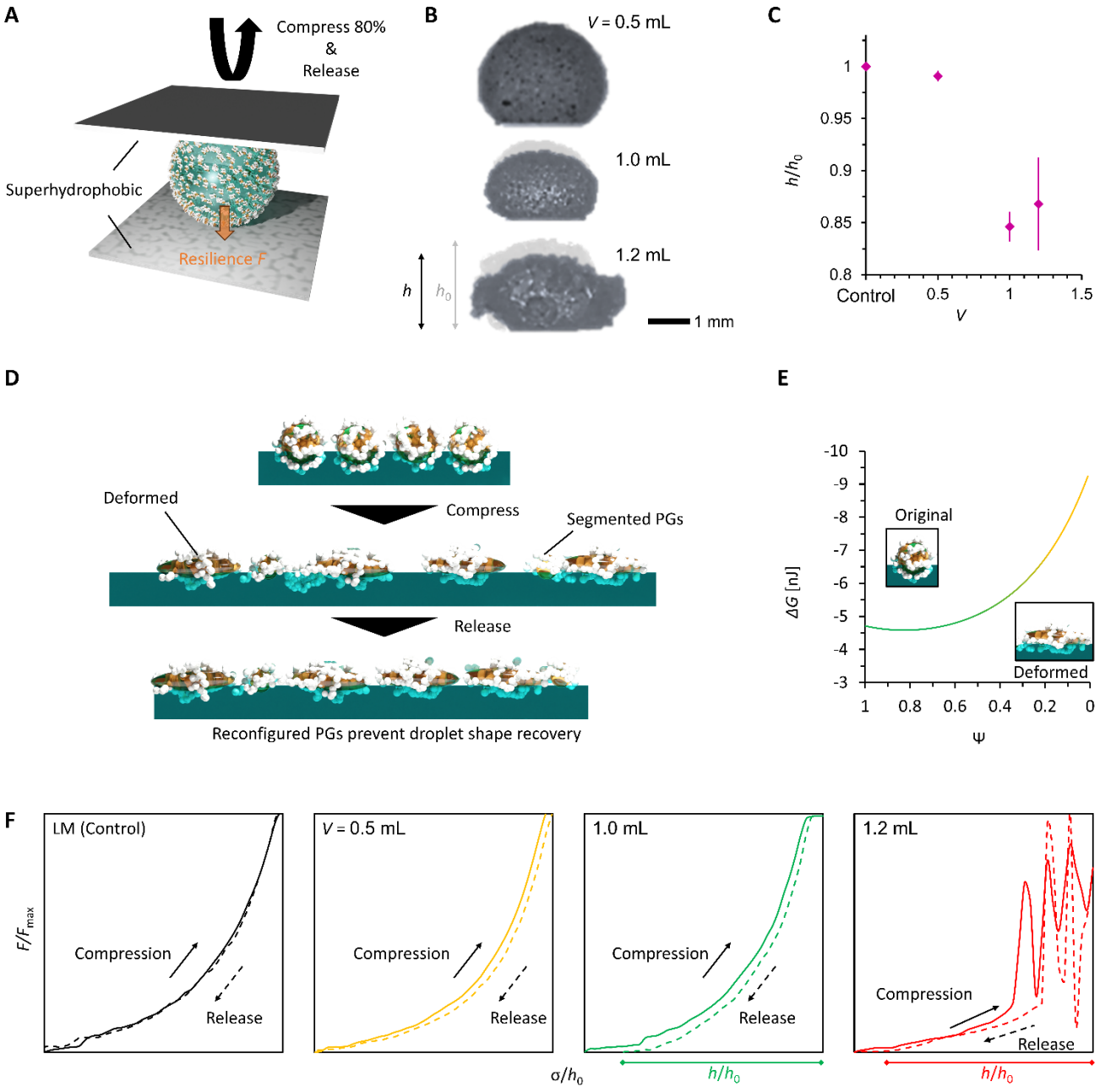

Figure 5. Shape reconfigurability of PGLMs. (A) Scheme of the compression-release conditions of PGLM. The compressing plate is superhydrophobized to prevent breakage of PGLM. (B) Shape change through the 80% compression for different PGLM. The PGLM height varied from h_0 to h. (C) Height change of PGLMs through the compression. (D) Scheme of possible PG contribution on incomplete recovery of PGLMs. (E) Estimated decrease in ΔG in PG sphericity decreased. (F) Hysteresis of resilience in compression and release of PGLM.

that the surface friction increases with V from 0 to 0.1 mL and 0.1 to 0.5 mL. The increased surface friction from 0 to 0.1 mL means the PDMS modification onto the nanoparticle surface. The significant α jump between V = 0.1 and 0.5 mL means a drastic change in grain surface properties, depending on whether the liquid PDMS sticks to the grains. In V > 0.5 mL, α exponentially decreased with V, while the sticky liquid PDMS fraction on the grain is expected to increase. The decreased α is because the structural change D and Ψ with V dominates over α rather than the surface friction. The α of PGs was not increased even after two months in a glass bottle (**Figure S4**), which indicated that the spill of the PDMS in PG did not occur, at least on a monthly scale.

In Figure 4, we evaluated the compression stability of PGLMs. PGLMs were prepared by covering 10 μL water droplet with PG and

compared with control LM using AEROSIL® RY300. PGs densely covered the water droplet surface and worked to delay the water evaporation (**Figure S5**). A PGLM or LM was compressed at a speed of 0.1 mm/s between two hydrophilic glass plates and measured the compression ratio σ versus resilience *F* using microbalance (**Figure 4A**). The side-view compression behaviors are shown in **Movie S1,** and **Figure 4B** captured those just before the breakage. We find PGLMs had superior compression stability to a control LM as their critical compression ratio is higher than the control. However, the critical compression ratio was not significantly different between PGLMs despite the change in the roughness. The PGLMs break down with cracks on their surface (**Figure 4B**), while the control LM has no crack throughout the compression. The cracking suggests the fracture of the PG network at the surface, which might increase the necessary work of rupture of the PGLM compared to the control LM. The networked shell feature may arise from the capillary bridging of nanoparticles via liquid PDMS.[20] **Figure 4C** plotted the σ-*F* curve in the log-log scale obtained from **Figure S6**. We obtained the power law $F \sim \sigma^{3/2}$ from the slope of LM and PGLMs in V = 0.5 and 1.0 mL. This power law explains the elastic sphere compression force, known as the Hertz model.[21] Thus, the resilience mainly comes from the quasi-elasticity of the water,[22] not the variation in the shell elasticity. In contrast, PGLMs in V = 1.2 mL exhibited a non-monotonic σ-*F* curve. Classically, when the LMs break down, their resilience drastically decreases. A similar tendency is observed for PGLMs in V = 0.5 and 1.0 mL, but not in V = 1.2 mL in comparing **Figure 4B** with **Figure 4C**. Instead, the resilience drastically increased after breakage, resulting from the PGs' viscous energy dissipation in shape rearrangement (disconnecting/reconnecting of liquid PDMS capillary bridge), which is confirmed by the side-view microscopic observation (**Figure 4D**) and non-monotonic resilience curve in compressing the PG (**Figure S7**). For V = 1.2 mL, unlike the cases of V = 0.5 and 1.0 mL, the size of the PG particles comprising the PGLM is not negligibly small compared with that of the PGLM. Therefore, we assume that the large fluctuation in resilience at the high compression area (the pink highlighted region in **Figure 4C**) is attributed to the contribution from the compression stress for reconfiguration of the PG network (**Figure 2F**). Especially, the PGs' reconfiguration mainly occurred on the side of the PGLM as seen in **Movie S1**. This is because the force chain connecting PGs and the glass plate is formed on the side of the PGLMs, and transmit compression force to PGs.

To convince the reconfiguration effect of PGLM, we investigated the hysteresis during the compression and release of the PGLMs in **Figure 5**. In this experiment, PGLMs were sandwiched between superhydrophobically coated glass plates, experienced 80% compression and release, and resilience was monitored (**Figure 5A**). On superhydrophobic surfaces, LMs are free from breakage owing to the reversible transition between particle adsorbed and water surface exposed states,[23] which enables the monitoring of compression hysteresis without breakage. The side-view of the compression/releasing behavior is shown in **Movie S2**; and **Figure 5B** highlights the shape change through the compression/releasing process, indicating the V-dependent distortion of PGLMs. The distortion was quantified by the height ratio of PGLMs before and after the compression (h/h_0), as shown in **Figure 5C**. The PGLMs with V = 1.0 and 1.2 mL were distorted through compression ($h/h_0 \approx 0.85$), while control LM and PGLM with V = 0.5 mL kept their original shapes, i.e., $h/h_0 \approx 1$. Since liquid surface tension is not changed by compression, the PGLMs' distortion is due to the structural change in the PG shell. As shown in **Figure 5D**, the surface area of the LM increases when it is compressed. In the case of a classical LM, the gap between the particles increases as it deforms. When the LM is released, the gap disappears and returns to its original shape. In contrast, when PGLM is compressed, the PG layer is reconfigured on the water surface, and the contact area between PG and water changes dynamically. The space between particles becomes smaller than between non-deformed particles, and the PGLM cannot return to its original shape when released. The reconfiguration is owing to the shape deformation, rearrangement, and/or segmentation of the PG shell (**Figure 2F**). The rearrangement decreases the PG absorption energy with increased water–PG contact area. For example, **Figure 5E** numerically studied the effect of PG shape deformation on absorption energy. Simple modeling of PG to be the prolate spheroid shape and its Young water contact angle being 90° (see **Figure S8** and **Note S1** for details), Gibbs Energy change Δ*G* through PG adsorption to water surface from airside can be estimated as:

$$\Delta G \approx \gamma_L \pi D^2 \left[\frac{1-\Psi}{1+\Psi}\right][-1+\Psi^2\{1-\tanh^{-1}(1-\Psi^2)\}]$$

, where $\gamma_L \approx 72.8$ mJm^{-2} is water surface energy. Figure 5E displayed Δ*G* variation as a function of the PG sphericity Ψ Since Ψ reflects the deformation degree, we can explain Δ*G* decreases with the PG deformation. This means that compression improves the PG shell stability, which is analogous to self-toughening materials.[24]

Figure 5F plotted normalized resilience during the compression and release. The hysteresis of PGLMs looks more significant than the control LM, depending on the shell reconfiguration degree. The

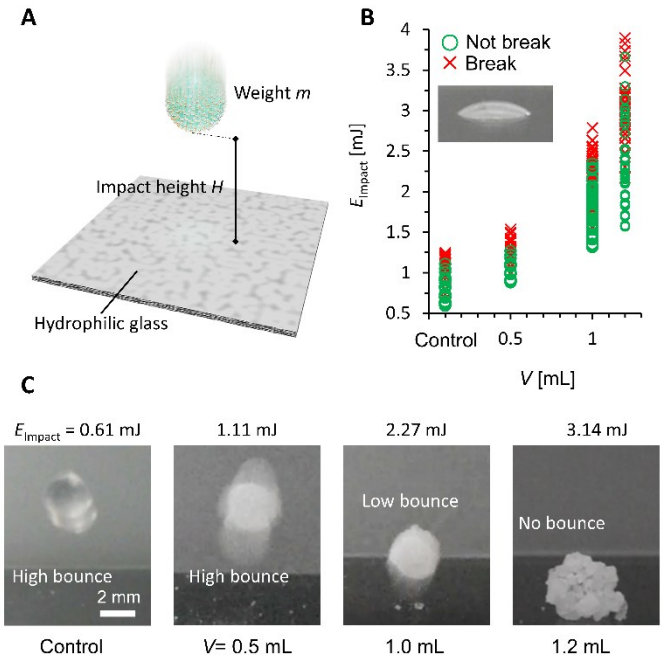

Figure 6. (A) Scheme of impact test. (B) Impact stability under different impact energy conditions. (C) Bouncing behavior of impacting LM and PGLMs.

fluctuation in resilience in V = 1.2 mL corresponds to the energy dissipation of PG. The resilience becomes zero for PGLMs with V = 1.0 and 1.2 mL before the plates reach the initial compression height ($\sigma < h_0$). The mechanical properties of PGLMs shown in **Figures 4** and **5** do not appear in classical (soft) solid particles-based LMs.

Finally, we studied the impact stability of the PGLMs (**Figure 6A**). We dropped the PGLM with 10μL water to the hydrophilic glass from the impact height h, the distance between the glass surface and the bottom of the PGLMs. Assuming that the potential energy of PGLMs is fully converted to kinetic energy, the impact energy is given by $E_{\mathrm{Impact}} \approx mgh$, where m is the weight of the PGLM and g is the gravitational acceleration constant. We judged the PGLMs' breakage depending on whether they kept spherical or adhered to the glass surface. The result is summarized in **Figure 6B**. We find that the PGLMs exhibited significantly superior impact resistance to control LM, and their critical impact energy increased with V. Since the power size between PG (V = 0.5 and 1.0 mL) and control is not significantly different, the increased impact stability is mainly contributed by the viscous dissipation of the liquid PDMS. In the case of PGLM (V = 1.2 mL), the grain size is significantly greater than the compared samples. With the increase of the powder size, the substrate−inner water gap length and particle attraction can be increased. [25] The highest impact stability for PGLM (V = 1.2 mL) may be owing to the synergetic effect of viscous dissipation and size growth. **Figure 6C** and **Movie S3** displays the bouncing behaviors of the impact LM and PGLMs. Due to viscous dissipation of impact energy, impacted PGLMs with V = 1.0 or 1.2 mL exhibited low or no bouncing, while those with V = 0.5 mL or control LM apparently bounced off at lower E_{Impact}. Moreover, we summarized the compression/impact stability between classical LMs and PGLMs in **Table S1**, which supports the effectiveness of the viscous dissipation approach in improving the LM robustness.

In summary, PGLM exhibited superior compression/impact stability to classical LMs and shape reconfigurability caused by the viscoelastic feature of PGs. While LM design parameters are reaching a limit, this study establishes new design guidelines, including introducing sister fluid as a gel component. In our PGLMs, the sister liquid PDMS improved mechanical functions through viscoelastic effects and adaptive morphological changes of shells.[26] Sister fluids are not limited in PDMS, but functional fluids like ionic liquid, liquid metal, ferrofluid, liquid crystal, biofluid, phase change liquid, non-newtonian liquids, and other responsive fluids.[27–30] The synergetic effect of functional particles and liquids of PGs makes the PGLMs highly functional.

Author Contributions

M.T.: Conceptualization, Data curation, Formal Analysis, Funding acquation, Investigation, Methodology, Project administration, Supervision, Validation, Visualization, Writing-original draft, review and editing. R.T.: Data curation, Formal Analysis, Investigation, Methodology, Validation, Writing-original draft, review and editing.

Acknowledgement

The authors appreciate support from WPI-MANA. We thank Ms. Makiko Yabune and Ms. Michie Saito who supported this work. This work is supported by JST FOREST, and partially by JSPS KAKENHI (21H01643 and 23K18567) to M.T.

Conflicts of interest

There are no conflicts to declare.

Notes and references

1 M. Tenjimbayashi and K. Manabe, *Sci Technol Adv Mater*, 2022, **23**, 473–497.
2 A. Lafuma and D. Quéré, *Nat Mater*, 2003, **2**, 457–460.
3 M. Tenjimbayashi, T. Mouterde, P. K. Roy and K. Uto, *Nanoscale*, 2023, **15**, 18980–18998.
4 P. Aussillous and D. Quéré, *Nature*, 2001, **411**, 924–927.
5 S. Fujii, S. Yusa and Y. Nakamura, *Adv Funct Mater*, 2016, **26**, 7206–7223.
6 M. Tenjimbayashi and S. Fujii, *Small*, 2021, **17**, 2102438.
7 Y. Asaumi, M. Rey, K. Oyama, N. Vogel, T. Hirai, Y. Nakamura and S. Fujii, *Langmuir*, 2020, **36**, 13274–13284.
8 Z. Liu, X. Fu, B. P. Binks and H. C. Shum, *Langmuir*, 2015, **31**, 11236–11242.
9 M. Tenjimbayashi, Y. Watanabe, Y. Nakamura and M. Naito, *Adv Mater Interfaces*, 2020, **7**, 183–195.
10 Z. Zhao, C. Ling, D. Wang, J. Wang, J. Saczek, S. Pramana, S. Sridhar, J. Shang, B. B. Xu, D. C. W. Tsang, J. Chen and S. Wang, *Small*, 2020, **16**, 2002802.
11 Y. Timounay, O. Pitois and F. Rouyer, *Phys Rev Lett*, 2017, **118**, 1–5.
12 J. Saczek, X. Yao, V. Zivkovic, M. Mamlouk, D. Wang, S. S. Pramana and S. Wang, *Adv Funct Mater*, 2023, **33**, 2214840.
13 N. Barman, A. Shome, S. Kumar, P. Mondal, K. Jain, M. Tenjimbayashi and U. Manna, *Adv Funct Mater*, 2021, **31**, 2011198.
14 K. L. Thompson, M. Williams and S. P. Armes, *J Colloid Interface Sci*, 2015, **447**, 217–228.
15 P. K. Roy, B. P. Binks, E. Bormashenko, I. Legchenkova, S. Fujii and S. Shoval, *J Colloid Interface Sci*, 2020, **575**, 35–41.
16 K. Aono, K. Ueno, S. Hamasaki, Y. Sakurai, S. Yusa, Y. Nakamura and S. Fujii, *Langmuir*, 2022, **38**, 7603–7610.
17 T. Takei, R. Tomimatsu, T. Matsumoto, K. R. Sreejith, N.-T. Nguyen and M. Yoshida, *Polymers*, 2022, **14**, 4849.
18 N. Celik, S. Akay, F. Sahin, G. Sezer, E. Dagasan Bulucu, M. Ruzi, H. Butt and M. S. Onses, *Adv Mater Interfaces*, 2023, **10**, 1–12.
19 E. Jenner and B. D'Urso, *Appl Phys Lett*, 2013, **103**, 251606.
20 E. Koos and N. Willenbacher, *Science*, 2011, **331**, 897–900.
21 H. Butt, K. Graf and M. Kappl, *Physics and Chemistry of Interfaces*, Wiley, 2003.
22 S. Asare-Asher, J. N. Connor and R. Sedev, *J Colloid Interface Sci*, 2015, **449**, 341–346.
23 M. Tenjimbayashi, S. Samitsu, Y. Watanabe, Y. Nakamura and M. Naito, *Adv Funct Mater*, 2021, **31**, 1–8.
24 T. Matsuda, R. Kawakami, R. Namba, T. Nakajima and J. P. Gong, *Science*, 2019, **363**, 504–508.

25 Y. Asaumi, M. Rey, K. Oyama, N. Vogel, T. Hirai, Y. Nakamura and S. Fujii, *Langmuir*, 2020, **36**, 13274–13284.
26 J. Zhang, B. Chen, X. Chen and X. Hou, *Advanced Materials*, 2021, **33**, 2005664.
27 M. Kole and S. Khandekar, *J Magn Magn Mater*, 2021, **537**, 168222.
28 T. Daeneke, K. Khoshmanesh, N. Mahmood, I. A. de Castro, D. Esrafilzadeh, S. J. Barrow, M. D. Dickey and K. Kalantar-zadeh, *Chem Soc Rev*, 2018, **47**, 4073–4111.
29 T. Nakanishi, *Functional Organic Liquids*, Wiley, 2019.
30 G. Kaur, H. Kumar and M. Singla, *J Mol Liq*, 2022, **351**, 118556.